Locus cœruleus noradrenergic neurons phase-lock to prefrontal cortical and hippocampal infra-slow rhythms which synchronize with behavioral events

Liyang Xiang[1,2], Antoine Harel[1], Ralitsa Todorova[1], HongYing Gao[1], Susan J. Sara[1,3] & Sidney I. Wiener[1]

[1]Center for Interdisciplinary Research in Biology (CIRB), College de France, CNRS, INSERM, PSL Research University, Paris, France

[2]Zhejiang Key Laboratory of Neuroelectronics and Brain Computer Interface Technology, Hangzhou, China

[3]Department of Child and Adolescent Psychiatry, New York University Medical School, New York, NY, USA

Abstract

The locus cœruleus (LC) is the primary source of noradrenergic projections to the forebrain, and, in prefrontal cortex, is implicated in decision-making and executive function. LC neurons phase-lock to cortical slow wave oscillations during sleep. Such slow rhythms are rarely reported in awake states, despite their interest since they correspond to the time scale of behavior. Thus, we investigated LC neuronal synchrony with infra-slow rhythms in awake rats performing an attentional set-shifting task. Local field potential (LFPs) oscillation cycles in prefrontal cortex and hippocampus on the order of 0.4 Hz phase-locked to task events at crucial maze locations. Indeed, successive cycles of the infra-slow rhythm showed different wavelengths, and thus these are not periodic oscillations. Simultaneously recorded infra-slow rhythms in prefrontal cortex and hippocampus showed different cycle durations as well. Most LC neurons (including optogenetically identified noradrenergic neurons) recorded here were phase-locked to these infra-slow rhythms, as were hippocampal and prefrontal units recorded on the LFP probes. The infra-slow oscillations also phase-modulated gamma amplitude, linking these rhythms at the time scale of behavior to those coordinating neuronal synchrony. Noradrenaline, released by LC neurons in concert with the infra-slow rhythm, would facilitate synchronizing or resetting those brain networks, underlying behavioral adaptation.

Introduction

The brain coordinates activity among interconnected regions via coherent oscillatory cycles of excitation and inhibition (Womelsdorf, et al., 2007). This can facilitate communication among selected subsets of neurons, groups of neurons, and brain regions. Sensory stimuli or behavioral events can reset the phase of these oscillations (Canovier, 2016; Voloh & Womelsdorf, 2016), linking activity of multiple neurons to process information in concert. However, the principal brain rhythms studied in behaving animals are at the time scale of cell neurophysiological processes, which are much faster (on the order of tens and hundreds of milliseconds) than real life behavioral events, which typically occur at second and supra-second time scales. The brain has several mechanisms linking these two time scales, some of which involve the hippocampus (e.g., Banquet, et al., 2021) and associated networks, including the prefrontal cortex.

Little is known about brain rhythms that operate in this crucial behavioral time scale during awake behavior. The brain is indeed capable of generating rhythms on

the order of 0.1-1.0 Hz, although these have been principally characterized during sleep (Steriade, 1993). Furthermore, during sleep or under anesthesia, rat noradrenergic locus cœruleus (LC) and prefrontal cortical (Pfc) neurons are phase-locked to slow rhythms (Lestienne, et al., 1997; Eschenko, et al., 2012). LC stimulation exerts powerful influence on neurophysiological activity in Pfc and hippocampus (Hip; Berridge and Foote, 1991). LC actions in prefrontal cortex are implicated in vigilance, decision-making, and executive function, while in Hip they are associated with learning and processing contextual information (e.g., Wagatsuma, et al., 2018; Sara, 2009 for review). Since oscillations can coordinate activity in brain networks, we reasoned that there might also be rhythmicity on this behavioral time scale in awake animals, and investigated this possibility in rats performing a task engaging Pfc, Hip and LC (Oberto, et al., 2022; Xiang, et al., 2019). Such coordinated activity could provide a possible link between neuromodulation and oscillatory coordination of brain areas on the time scale of behavior.

Results

LC neuron phase-locking to prefrontal and hippocampal infra-slow rhythms

Rats equipped for chronic recordings alternated between visual and spatial discrimination tasks in an automated T-maze with return arms. Visual inspections of hippocampal (Hip) and prefrontal cortical (Pfc) local field potentials (LFPs) revealed infra-slow rhythms (Fig. 1A). These were rendered more salient by filtering the signal in a 0.1-1.0 Hz window (Fig. 1B). We applied an amplitude threshold to examine data from those periods when the infra-slow rhythm amplitude was elevated (Fig. 1C), and observed that LC neurons were phase-locked to Pfc, as well as Hip infra-slow LFP rhythms (n=21 out of 37, and 18 out of 37, respectively; Rayleigh test, $p<0.05$; Fig. 1D; for histology, see Fig. 2 of Xiang, et al., 2019).

The modal preferred infra-slow phase among these neurons was $0.35*\pi$ radians for Hip infra-slow and $0.15*\pi$ radians for Pfc infra-slow (Fig. 3; $p<0.05$, Rayleigh test). In one animal, noradrenergic LC neurons were identified optogenetically (see Methods), and most were phase locked to the infra-slow rhythms (n= 8 out of 11 for LFPs in both Pfc and Hip; Rayleigh test, $p<0.05$). (Since, apart from this high incidence, the LC neurons identified optogenetically as noradrenergic had responses similar to the others, they are all described together.) Another rat had a high incidence of infra-slow phase-locking by LC neurons (10/12 and 9/12 respectively for Hip and Pfc), while in the other two rats with LC recordings this was rare (1/8 and 1/8; 2/6 and 0/6). The reason for this variation is not clear, but could be related to the recordings having sampled different subpopulations of LC neurons (Chandler, et al., 2014).

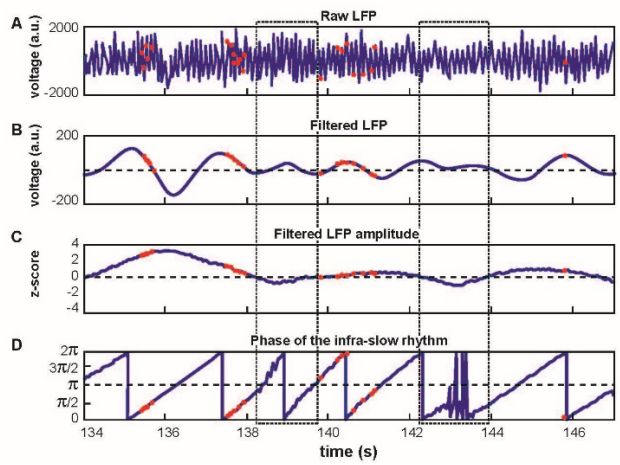

Figure 1. Calculation of LC spike phase relative to Hip or Pfc LFP. A) Unfiltered signal with theta oscillations dominating. B) The signal from A band-pass filtered at 0.1-1.0 Hz. Red dots indicate LC neuron action potentials in all panels. C) The amplitude of the signal in B was z-scored. Low amplitude oscillations were excluded from analyses according to an (arbitrary) criterion of $z\leq0$ (excluded zones are demarcated by the dotted rectangles). D) Phase of the filtered signal in B. Note that the LC spikes generally occur at phases between 0 and $\pi/2$ radians in this example. The discontinuities near 138.5 and 143 s correspond to excluded data, where phase could not be computed reliably.

Prefrontal and hippocampal infra-slow rhythms synchronized to maze events

The infra-slow rhythms were phase-locked to positions on the maze (Fig. 2; Supp. Fig. 1B). To quantify this phase-locking, the mean (± SEM) phase of the rhythm was plotted in peri-event time color plots (see Fig. 4 for examples) over all trials in 57 sessions from eight rats. 'Regular phase-locking' describes those periods when the SEM range was less than $0.75*\pi$ radians (see Fig. 4, middle column).

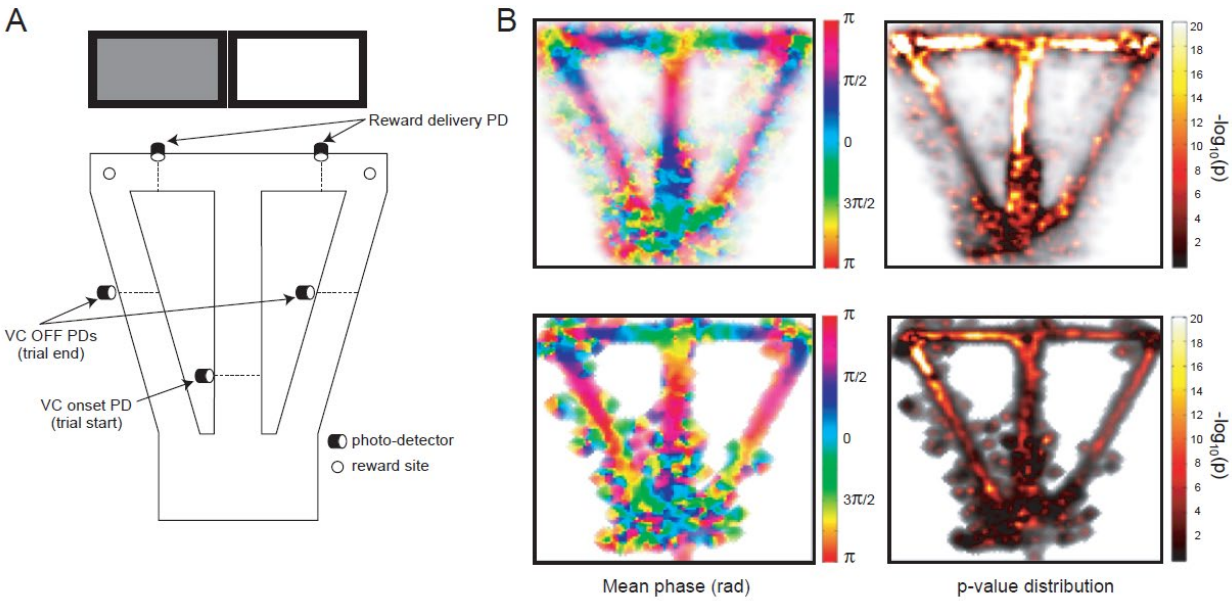

Figure 2. A) The automated behavioral task. When the trained rat crosses the central arm photodetector (VC onset PD), this triggers one of the two cue screens behind the reward arms to be lit in pseudo-random sequence. Crossing the appropriate reward delivery PD triggers a drop of sweetened water to arrive at the corresponding reward site. Crossing the VC OFF PD's on the return arms triggers the lit screen to be turned off. These three photodetector events are used to synchronize activity in subsequent Figures. B) Distribution of mean phase (left) and p-values of phase-locking (right; Rayleigh test) for Pfc infra-slow oscillations in pooled data from multiple sessions (top), and in an example session (bottom).

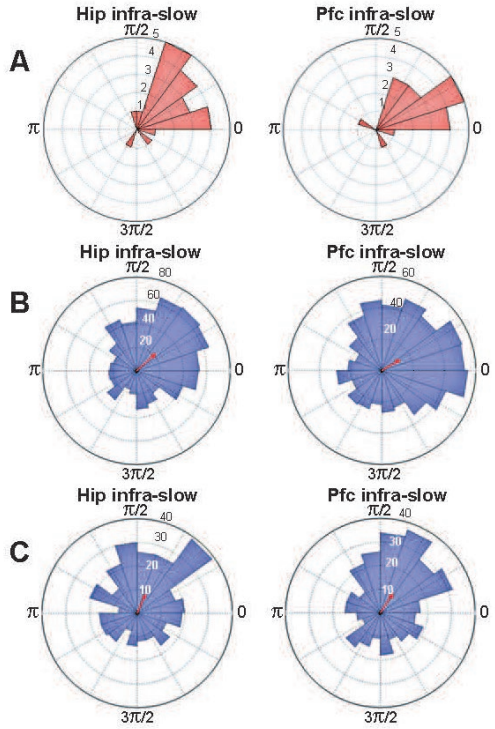

Figure 3. A) Distribution of preferred phases (i.e., phases of resultant vectors) for all LC neurons with spiking significant phase-locking to Hip and Pfc infra-slow rhythms. Radius values are numbers of neuron. B, C) Spike phase-locking to infra-slow rhythms from two example LC neurons. Radius values are spike counts. Red arrows represent resultant vectors.

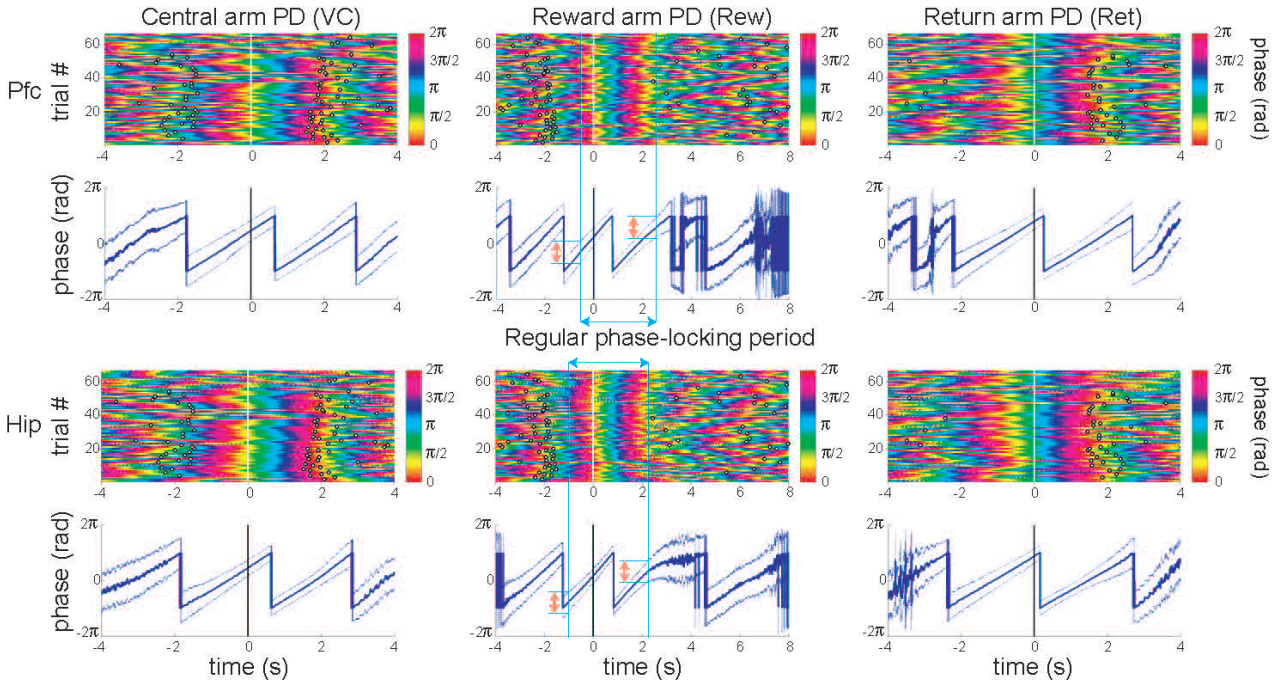

Figure 4. An example of simultaneous recordings of Pfc and Hip LFP infra-slow oscillations phase-locked to principal maze events, the PD crossings (at time zero). Each row of the color plots corresponds to a single trial and the phase of the infra-slow LFP is color-coded. Black rings correspond to the PD crossing prior to (left) or after (right) the event at zero for each plot. Note that the time scales vary among the events in order to display prior and subsequent PD's. The traces below show mean (± SEM) phase. In the middle column, the blue vertical bars and blue double-headed arrow illustrate the calculation of the range of regular phase-locking (defined here as the period with the arbitrary criterion of SEM range<0.75*π radians; pink double-headed arrows). Here, desynchronization (zones with large SEM ranges) and discontinuities in the mean phase result from inter-trial variability in speed and distance from the synchronization point. (PD - photodetector crossing). This is from the same session as the recording in Fig. 3B.

Infra-slow rhythms were phase-locked to the reward arm photodetector crossing (Rwd) in 51 of the recording sessions for Hip, and 46 sessions for Pfc (see Table 1). The other maze events had fewer incidences of regular phase-locking (Pfc return arm photodetector crossing, or Rtn: 11; Pfc central arm visual cue onset PD, or VC: 18; Hip Rtn: 18; Hip VC: 20). The mean phases at the respective PD crossings (when SEM≤0.75*π radians there) were 0.70*π and 0.24*π radians for Pfc and Hip Rtn, 0.25*π and 0.22*π radians for Pfc and Hip Rwd, and 0.19*π and 0.01*π radians for Pfc and Hip VC. The root-mean-square differences between Pfc and Hip mean phase (calculated pairwise by session) at the respective PD crossings were 0.14*π, 0.13*π and 0.12*π rad. The regular phase-locking could last from less than one to over 2.5 successive rhythmic cycles (Fig. 3, Supp. Figs. 1 and 2, see Table 1) and could continue from one event to the next (Fig. 4, Supp. Fig. 1). For PL Rwd and Hip Rwd, 30 and 37 sessions had durations of regular phase-locking lasting one or more cycles, respectively. These permitted quantification of the temporal duration of the cycles, which ranged from 2.0 to 2.6 s, the equivalent of 0.4 to 0.5 Hz. In the six cases of Rwd PD phase-locking which had a second complete cycle, the mean of the first was 2.3 s, while the second was lower, 2.0 s (pairwise t-test, p=0.0009, df=5). Thus, these are not regular periodic oscillations, but rather are consistent with phase-locking to task events. Pfc and Hip infra-slow rhythms sometimes resembled one another (e.g., Fig. 2). To compare them, sessions were classified as having Pfc and Hip regular phase-locking in the following ranges of cycles (see Table 1). In 17 of the 57 sessions, these numbers of cycles were different between Pfc and Hip for VC, Rwd and/or Rtn (e.g., Supp. Fig. 2). This indicates that it is unlikely that Pfc and Hip infra-slow rhythms are related by volume conduction.

The infra-slow rhythms were regularly phase-locked to two (in 24 sessions), or even all three (in 8 sessions)

different task events. Thus, they were not linked to any specific task-related behavior. To test whether infra-slow rhythms were triggered by rapid head movements, regression analysis compared the onset of regular phase-locking and times of peak acceleration, or deceleration around the Rwd PD crossings, and were not significant (R^2=0.034, p=0.49 and R^2=0.0056, p=0.80 respectively; df=15; see Supp. Fig. 3). Additionally, spatial distributions of speed and acceleration do not resemble the phase maps (Supp. Fig. 3). Moreover, in Xiang et al. (2019) we showed that LC neurons fire more during accelerations. Indeed, the periods with the greatest increase in LC activity were not those most frequent for the start of regular phase-locking (i.e., reset) of the infra-slow rhythm; rather phase-locking occurred most frequent ly to Rwd PD crossing (see above), where no consistent accelerations occurred (see Supp. Figs. 3 and 4). These results indicate it is unlikely that Pfc and Hip infra-slow rhythms are due to a biomechanical artifact, for example from locomotion or head rocking.

	Pfc Rtn	Pfc Rwd	Pfc VC	Hip Rtn	Hip Rwd	Hip VC
<1 cycle (n)	4	16	10	13	14	9
1 to 1.49 cycles (n)	6	20	6	3	28	8
1.5 to 1.99 cycles (n)	1	6	2	2	7	3
2 to 2.49 cycles (n)	0	4	0	0	1	0
2.5 to 3 cycles (n)	0	0	0	0	1	0
Mean cycle period (s)	2.48	2.22	2.05	2.62	2.45	2.32
Mean frequency (Hz)	0.40	0.45	0.49	0.38	0.41	0.43

Table 1. Characterization of periods in sessions with regular phase-locking to infra-slow LFP oscillations. Note that for the six cases of two or more cycles, only data from the first cycle were counted for mean cycle period and frequency. Cycles are only counted in the period from the previous trial event to the next one, even though infra-slow rhythms could continue before or after (cf., Fig. 4, Supp. Fig. 1).

Coordination of neuronal activity across time scales

In the four sessions where Hip and Pfc neurons could be discriminated from the LFP electrodes, most were also modulated by infra-slow rhythms (Pfc LFP modulated 6/12 Pfc units and 8/11 Hip units; Hip LFP modulated 8/12 Pfc units and 8/11 Hip units; Rayleigh test p<0.05). The LC neurons had relatively consistent phases with respect to the two infra-slow rhythms (Fig. 3). LC neurons could be phase-locked to oscillations in the delta frequency range (1-4 Hz) in Pfc (n=15/37) and Hip (11/37) as well as theta (5-10 Hz; 7/37 and 5/37 respectively) for Pfc and Hip (Supp. Table 1). While phase-locking of LC neurons to gamma (40-80 Hz) was rare (n=2 for both structures' LFPs), the infra-slow rhythm did modulate the amplitude of their gamma oscillations at 35-45 Hz (Fig. 5).

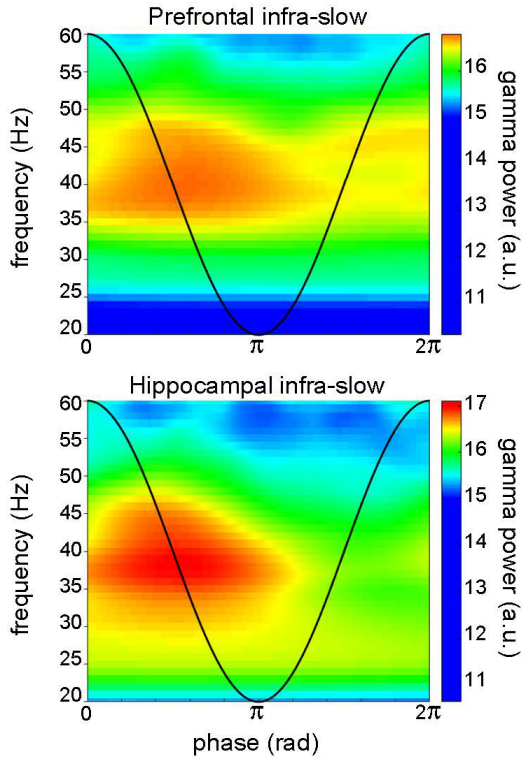

Figure 5. Example of infra-slow modulation of gamma rhythm LFP in Pfc (top) and Hip (bottom).

Discussion

LFP oscillation cycles on the order of 0.4 Hz in prefrontal cortex and hippocampus were phase-locked to task events at crucial points on the maze. Successive cycles had different cycle lengths, indicating that these are not periodic oscillations. Simultaneous recordings in prefrontal cortex and hippocampus could have different cycle lengths as well. Over half of the LC neurons recorded here were phase-locked to these infra-slow prefrontal cortical and hippocampal LFPs, including optogenetically identified noradrenergic neurons. Hippocampal and prefrontal units were also phase-locked to the infra-slow oscillations.

This is consistent with previous work showing neuronal activity adapting to the time scale of behavioral events. For example, in behavioral tasks with delays, several brain structures show "time cell" activity: neurons with sequential "tiling" activity lasting on the order of several seconds. These periods can expand or contract depending upon the duration of task-imposed intervals (MacDonald, et al., 2011). We speculate that this infra-slow rhythm may originate in the hippocampal-prefrontal system since neuro-physiological activity there tracks time intervals on the order of several seconds based upon regularities in temporal structure of behavioral or environmental events.

Steriade, et al. (1993) observed infra-slow (0.3-1.0 Hz) rhythms in neocortical activity in anesthetized and naturally sleeping cats. Eschenko et al (2012) showed that LC neuronal activity in sleeping rats is synchronized with the sleep slow wave cycle (1 Hz) and is out of phase with Pfc neuronal activity. Similarly, in rats under ketamine anesthesia, there is a negative correlation between activity of LC NE neurons and prefrontal neurons, when neuron activation oscillates at ~1 Hz (Sara and Hervé-Minvielle 1995; Lestienne, et al. 1997). While these slow cycles of UP-DOWN state transitions are not generally observed in awake animals, this does demonstrate that these structures can coordinate their activity at this time scale. Thus the LC could also be associated with the Pfc-Hip in the origin, maintenance and communication of behaviorally relevant infra-slow rhythms in the brain. Further work is required to elucidate the respective roles of these structures in these processes.

In the awake state, there is evidence for infra-slow neural processing although this was not observed as rhythms per se. Molter, et al. (2012) observed a 0.7 Hz modulation of the power of theta rhythm recorded in rat Hip. This 0.7 Hz modulated Hip neuronal activity during sleep, as well as during behavior in a maze, a running wheel, and an open field. Positions on a figure-8 maze corresponded to specific phases of this modulatory rhythm, similar to the infra-slow rhythm recorded here. (Their filter settings excluded 0.7 Hz rhythms and thus this could not be directly measured in that work.) In Molter et al. (2012), the 0.7 Hz modulation of the power of the theta slow modulation was locked at π radians to junction points in the maze (their Figure 7B), where accelerations might be expected. However, they found no overall correlation between phase and acceleration.

Villette, et al. (2015) used calcium imaging to observe CA1 pyramidal cells in head fixed mice moving in the dark on a non-motorized treadmill. They found that different neurons fired sequentially in cycles at the same time scale as the infra-slow oscillations observed here. Furthermore, the cycles could occur singly, or consecutively in groups of two or three. The authors interpreted this as representing an intrinsic metric for representing distance walked. This resembles time cell activity (Pastalkova et al., 2008; MacDonald et al., 2011) evoked above, where the length of the cycle extends to the time scale of the ongoing task (Kraus, et al., 2013; Ravassard, et al., 2013). The 2 to 5 s durations of the cycles in the Villette, et al. (2015) study may represent a default value since their task had no temporal structure. This is on the order of the time scale of the infra-slow rhythm recorded here, and the variable numbers of cycles they observed might flexibly adapt to the positions of task-relevant events to lead to the results found here.

The present observations of phase-locking of LC neurons to infra-slow rhythms in hippocampus could ostensibly be due to independent synchrony of the infra-slow rhythms and the LC neurons to task events. However, the LC neurons showed phase preferences in the infra-slow rhythms in data pooled over multiple task events. We did not observe any simple relation between infra-slow rhythms and motor events (e.g., as we showed for LC neurons with acceleration or deceleration by Xiang, et al., 2019) since regular phase-locking could start before (Supp. Fig. 1) or after the same task events in different sessions (not shown) and continue over periods including a variety of associated behaviors.

The phase-locking of LC neurons to infra-slow rhythms in Hip and Pfc, as well as to oscillations in the delta, theta and gamma frequency bands could reveals coordinated neuronal processing within a unified temporal framework. The scale of this corresponded to the temporal and spatial regularities characterizing the current behavioral patterns. Cross-frequency coupling could serve as a mechanism to link processing at different time scales. This could facilitate both 'Communication through coherence' (CTC, Bosman et al., 2012; Fries, 2005) and 'Binding by synchrony' (Eckhorn, et al., 1990; Engel, et al., 1999; Buehlmann and Deco, 2010). Thus, infra-slow rhythms would serve as a scaffold to link the time scales of dynamics of neuronal processes to those of behavior and cognitive processes. Noradrenaline, released by LC neurons in concert with the infra-slow rhythm, would participate in synchronizing or resetting those brain networks underlying behavioral adaptation to these events (Bouret & Sara, 2005; Sara & Bouret, 2012).

Materials and Methods

All experiments were carried out in accordance with local (Comité d'éthique en matière d'expérimentation animale no. 59), institutional (Scientific Committee of the animal facilities of the Collège de France) and international (US National Institutes of Health guidelines; Declaration of Helsinki) standards, legal regulations (Certificat no. B751756), and European/national requirements (European Directive 2010/63/EU; French Ministère de l'Enseignement Supérieur et de la Recherche 2016061613071167) regarding the use and care of animals. The data here are from experiments described in Xiang, et al. (2019) and further details can be found there.

Animals

Four male Long-Evans rats (Janvier Labs, Le Genest-Saint Isle France; weight, 280–400 g) were maintained on a 12 h:12 h light-dark cycle (lights on at 7 A.M.). The rats were handled on each workday. To motivate animals for behavioral training on the T maze, food was restricted to 14 g of rat chow daily (the normal daily requirement) while water was partially restricted except for a 10–30 min period daily to maintain body weight at 85% of normal values according to age. Rats were rehydrated during weekends.

The automated T maze with return arms

The behavoral task took place in an elevated automated T-maze (see Fig. 1) consisting of a start area, a central arm, two reward arms and two return arms which connected the reward arms to the start area. Small wells at the end of each reward arm delivered liquid reward (30 µl of 0.25% saccharin solution in water) via solenoid valves controlled by a CED Power1401 system (Cambridge Electronic Design, Cambridge, UK) with a custom-written script. Visual cues (VCs) were displayed on video monitors positioned behind, and parallel to the two reward arms. The VCs were either lit or dim uniform fields. Photodetectors detected task events and triggered cues and rewards via the CED Spike2 script. The sequence of left/right illumination of screens was programmed according to a pseudorandom sequence.

Viral vector preparation and injection

The Canine Adenoviral vector (CAV2-PRS-ChR2-mCherry) was produced at the University of Bristol using previously described methods (Li, et al., 2016). This CAV2 viral vector expresses channelrhopsin-2 (ChR2) under the control of PRSx8 (synthetic dopamine beta-hydroxylase promoter), which restricts the expression of the transgene to noradrenergic (NA) neurons (Figure VI.1a in Hwang, et al., 2001; also see Hickey, et al., 2014) In one rat (R328), 4 months before the electrode implant surgery, CAV2-PRS-ChR2-mCherry was injected into the right LC while the rat was anesthetized with sodium pentobarbital (40 mg⁄kg, with 5 mg sodium pentobarbital as a supplement every hour) intraperitoneally. The site corresponding to LC position was marked on the exposed skull for injection in right LC (AP ~3.9 mm relative to lambda, ML ~1.2 mm), and a trephine was made (~2 mm diameter). A micropipette (calibrated in 1 µl intervals, Corning Pyrex) with a tip diameter of 20 µm was connected to a Hamilton syringe, and backfilled with 1 µl of the diluted viral vectors. Microinjections of 0.33 µl were made into the LC (AP -3.8~-4 mm relative to lambda, ML 1.1-1.2 mm, with a 15° rostral tilt) at three sites dorsoventrally (5.2, 5.5, 5.7 mm below the brain surface). The pipette was left at each depth for an additional 3-5 min before moving down to the next site. When the injection was finished, the trephine hole was covered with sterilized wax and the scalp was sutured. The rat was observed until recovery and was then singly housed.

Electrode and optrode implants

Following VC task pre-training, at least one day before surgery, rats were returned to ad libitum water and food. General surgical preparation is described in

the previous section. Moveable tungsten microelectrodes (insulated with epoxylite®, impedance = 2-4 MΩ, FHC Inc, USA) were used for LC recordings. A single microelectrode, or two or three such electrodes glued together was implanted at AP -3.8-4 mm relative to lambda, and ML 1.1-1.2 mm, with a 15° rostral tilt. A stainless steel wire (Teflon coated, diameter=178 µm, A-M systems Inc) implanted in the midbrain area about 1-2 mm anterior to the LC electrode tip served as a fixed LC reference electrode, permitting differential recording. The rat with the virus injection (R328) was implanted with an optrode made of a tungsten microelectrode (insulated with epoxylite, impedance = 2-4 MΩ, FHC Inc, USA) glued to a 200 µm optic fiber implant with a ferrule (0.37 numerical aperture, hard polymer clad, silica core, multimode, Thorlabs), with tip distances 1 mm apart (the electrode was deeper). The optic fiber implant and optic fiber cables were constructed at the NeuroFabLab (CPN, Ste. Anne Hospital, Paris. Two screws (diameter = 1 mm, Phymep, Paris) with wire leads were placed in the skull above the cerebellum to serve as ground. LC electrodes were progressively lowered under electrophysiological control until characteristic LC spikes were identified (located ~ 5-6 mm below the cerebellar surface, see Xiang, et al., 2019 for details). For the virus-injected rat, LC spikes could also be identified by responses to laser stimulations (described below). Following implantation, the microelectrode was fixed to a micro-drive allowing for adjustments along the dorsal-ventral axis. The headstage was fixed to the skull with dental cement, and surrounded by wire mesh for protection and shielding. After the surgery, animals were returned to their home cages for at least one-week recovery with ad libitum water and food and regular observation.

Electrophysiological recordings

Rats were then returned to dietary restriction. The movable electrodes were gradually advanced until a well-discriminated LC unit was encountered and then all channels were recorded simultaneously while the rat performed in the T maze. If no cells could be discriminated, the electrodes were advanced and there was at least a 2 h delay before the next recording session.

For daily online monitoring of LC spikes, pre-amplified signals were filtered between 300-3000 Hz for verification on the computer screen (Lynx-8, Neuralynx, Bozeman, MT, USA) and also transmitted to an audio monitor (audio analyzer, FHC). For recordings, brain signals were pre-amplified at unity gain (Preamp32, Noted Bt, Pecs, Hungary) and then led through a flexible cable to amplifiers (x500, Lynx-8, Neuralynx) and filters (0.1-9 kHz, Lynx-8, Neuralynx). Brain signals were digitized at ~20 kHz using CED Power1401 converter and Spike2 data acquisition software. The LC unit activity was identified by: 1) spike waveform durations ≥0.6 ms; 2) low average firing rate (1-2 Hz) during quiet immobility; 3) brief responses to unexpected acoustic stimuli followed by prolonged (around 1 s) inhibition; 4) for the virus-injected rat (R328), LC units were verified by responses to laser stimulation. A laser driver (Laserglow Technologies, Canada, wavelength 473 nm) was controlled by signals from a stimulator (Grass Technologies, USA, Model SD9). Light intensity from the tip of optic fiber was measured by a power meter (Thorlabs, Germany, Model PM100D). If unit firing was entrained to the pulses with an increased rate (to at least twice the baseline firing rate) averaged over all the stimulations, they were considered to be noradrenergic LC units.

A light emitting diode (LED) was mounted on the cable that was plugged into the headstage. This was detected by a video camera mounted above the T-maze and transmitted to the data acquisition system at a sampling rate of ~30 Hz for the purpose of position tracking.

Tissue processing

After all recording experiments, electrolytic lesions (40 µA, 10 s cathodal current) were made at the tip of the electrodes. Brain slices were cut coronally at a thickness of 40 µm with a freezing microtome and were collected in cold 0.1 M PB for Nissl staining. Recordings at sites with reconstructed electrode positions outside LC proper were excluded from analysis. For fluorescent immunohistochemistry, sections were then incubated in primary antibodies overnight at 4°C in darkness with both chicken anti-tyrosine hydroxylase (TH) antibody (1:500, Abcam) and mouse anti-mCherry antibody (1:200, Ozyme) in PBS containing 0.1% Triton X-100 and 3% NGS. After three 5 min rinses in PBS, sections were then incubated with secondary antibodies in PBS containing 3% NGS for 1h at RT in darkness. Secondary antibodies used in this study were Alexa Fluor 488 goat anti-chicken IgG (1:3000, Life

Technologies) and Alexa Fluor 546 goat anti-mouse IgG (1:3000, Life Technologies).

Signal processing, spike sorting and data analyses

For off-line spike detection of LC activity in three of the rats, the wide-band signals were converted and digitally high-pass filtered (nonlinear median-based filter). Waveforms with amplitudes passing a threshold were extracted, and then subjected to principal component analysis (PCA). All of these processes were performed with NDManager (Hazan, et al., 2006). Spikes were sorted with a semi-automatic cluster cutting procedure combining KlustaKwik (KD Harris, http://klustakwik.sourceforge.net) and Klusters (Hazan, et al., 2006). Spikes with durations less than 0.6 ms were rejected. In one rat (R311) the LC signal was filtered from 300-3000 Hz during recording, and the spike sorting was performed with Spike2 software (which employs a waveform template matching algorithm). Most data analyses were performed using Matlab (R2010a) with the statistical toolbox FMAToolbox (developed by M. Zugaro, http://fmatoolbox.sourceforge.net) and scripts developed in the laboratory as well as some statistical analyses performed with Microsoft© Excel©. The latter application's calculated the regressions (passing through the origin) between the onset of regular phase-locking and times of peak acceleration or deceleration, and p-values were taken from https://www.socscistatistics.com. This analysis was performed only for Reward Arm PD synchronized data when the prior Central Arm PD mean phase data had no regular phase-locking (to avoid confounds and have sufficiently large data set).

Acknowledgements

Thanks to Professor Anthony E. Pickering for providing the virus and related advice. Thanks to Dr. Michaël Zugaro for helpful suggestions and help with analyses and computing, Drs. A Sirota and X Leinkugel for helpful discussions, and France Maloumian for help with figures. L.X. was supported by a fellowship from the China Scholarship Council (CSC). The Labex Memolife and Fondation Bettencourt Schueller provided support.

Competing interests

The authors declare that they have no competing interests.

References

Berridge CW, Foote SL. (1991) Effects of locus coeruleus activation on electroencephalographic activity in neocortex and hippocampus. J Neurosci. 11(10):3135-45. doi: 10.1523/JNEUROSCI.11-10-03135.1991

Bosman CA, Schoffelen J-M, Brunet N, Oostenveld R, Bastos AM, Womelsdorf T, Rubehn B, Stieglitz T, De Weerd P, Fries P. (2012) Attentional stimulus selection through selective synchronization between monkey visual areas. Neuron. 75:875–888. doi: 10.1016/j.neuron.2012.06.037.

Bouret S, Sara SJ. (2005) Network reset: a simplified overarching theory of locus coeruleus noradrenaline function. Trends Neurosci. 28(11):574-82. doi: 10.1016/j.tins.2005.09.002

Buehlmann A, Deco G. (2010) Optimal information transfer in the cortex through synchronization. PLoS Comput Biol 6. doi: 10.1371/journal.pcbi.1000934

Canavier CC. (2015) Phase-resetting as a tool of information transmission. Curr Opin Neurobiol. 31:206-213. doi:10.1016/j.conb.2014.12.003

Chandler DJ, Gao WJ, Waterhouse BD. (2014) Heterogeneous organization of the locus coeruleus projections to prefrontal and motor cortices. Proc Natl Acad Sci (U. S. A.) 111(18):6816-21. doi: 10.1073/pnas.1320827111.

Eckhorn R, Reitboeck HJ, Arndt M, Dicke P (1990) Feature linking via synchronization among distributed assemblies: Simulations of results from cat visual cortex. Neural Comput 2:293–307. https://doi.org/10.1162/neco.1990.2.3.293

Engel AK, Fries P, König P, Brecht M, Singer W (1999) Temporal binding, binocular rivalry, and consciousness. Conscious Cogn 8:128–51.

Eschenko, O, Magri C, Panzeri S, Sara, SJ (2012) Noradrenergic neurons of the cocus coeruleus are phase-locked to cortical Up-Down States during sleep. Cerebral Cortex 22(2):426-43. doi:10.1093/cercor/bhr121

Fries, P. A. (2005) A mechanism for cognitive dynamics: neuronal communication through neuronal coherence. Trends Cogn Sci 9:474–80. doi: 10.1016/j.tics.2005.08.011.

Hazan L, Zugaro M, Buzsáki G (2006) Klusters, NeuroScope, NDManager: A free software suite for

neurophysiological data processing and visualization. J. Neurosci. Meth. 155, 207–216. doi: 10.1016/j.jneumeth.2006.01.017.

Hickey L, Li Y, Fyson SJ, Watson TC, Perrins R, Hewinson J, Teschemacher AG, Furue H, Lumb BM, Pickering AE (2014) Optoactivation of locus ceruleus neurons evokes bidirectional changes in thermal nociception in rats. J Neurosci 34: 4148–4160. DOI: 10.1523/JNEUROSCI.4835-13.2014

Hwang DY, Carlezon WA, Isacson O, Kim KS (2001) A high-efficiency synthetic promoter that drives transgene expression selectively in noradrenergic neurons. Human Gene Ther 12: 1731–1740. doi: 10.1089/104303401750476230.

Kraus BJ, Robinson RJ, 2nd, White JA, Eichenbaum H, Hasselmo ME (2013). Hippocampal "time cells": time versus path integration. Neuron 78: 1090–1101. doi: 10.1016/j.neuron.2013.04.015.

Lestienne R, Hervé A, Robinson D, Brios L, Sara SJ (1997) Slow oscillations as a probe of the dynamics of the locus coeruleus-frontal cortex interaction in anesthetized rats. J. Physiology (Paris) 91, 273-284. doi: 10.1016/s0928-4257(97)82407-2.

Li, Y. Hickey L, Perrins R, Werlen E, Patel AA, Hirschberg S, Jones MW, Salinas S, Kremer EJ, Pickering AE (2016) Retrograde optogenetic characterization of the pontospinal module of the locus coeruleus with a canine adenoviral vector. Brain Res. 1641(Pt. B): 274–290. doi: 10.1523/JNEUROSCI.4835-13.2014

MacDonald, C., Lepage, K., Eden, U., Eichenbaum, H. (2011) Hippocampal "time cells" bridge the gap in memory for discontiguous events. Neuron 71(4):737–749. doi: 10.1016/j.neuron.2011.07.012.

Molter C, O'Neill J, Yamaguchi Y, Hirase H, Leinekugel X (2012) Rhythmic modulation of theta oscillations supports encoding of spatial and behavioral information in the rat hippocampus. Neuron 75:889–903. doi: 10.1016/j.neuron.2012.06.036

Oberto VJ, Boucly CJ, Gao H, Todorova R, Zugaro MB, Wiener SI. (2022) Distributed cell assemblies spanning prefrontal cortex and striatum. Curr Biol. 32(1):1-13.e6. doi: 10.1016/j.cub.2021.10.007

Pastalkova E, Itskov V, Amarasingham A, and Buzsáki G (2008). Internally generated cell assembly sequences in the rat hippocampus. Science 321(5894):1322-7. doi: 10.1126/science.1159775.

Ravassard P, Kees A, Willers, B, Ho D, Aharoni D, Cushman J, Aghajan ZM, Mehta MR (2013) Multisensory control of hippocampal spatiotemporal selectivity. Science 340:1342–1346. doi: 10.1126/science.1232655

Sara SJ (2009) The locus coeruleus and noradrenergic modulation of cognition. Nat Rev Neurosci. 10(3):211-23. doi: 10.1038/nrn2573.

Sara SJ, Bouret S. (2012) Orienting and reorienting: the locus coeruleus mediates cognition through arousal. Neuron 76(1):130-41. doi: 10.1016/j.neuron.2012.09.011.

Sara SJ, Hervé-Minvielle A (1995) Inhibitory influence of frontal cortex on locus coeruleus neurons PNAS. 92:6032-6036. doi: 10.1073/pnas.92.13.6032.

Steriade M, Contreras D, Curro Dossi R, Nunez A (1993) The slow (<1 Hz) oscillation in reticular thalamic and thalamocortical neurons: scenario of sleep rhythm generation in interacting thalamic and neocortical networks. J Neurosci. 13:3284-3299. doi: 10.1523/JNEUROSCI.13-08-03284.1993.

Villette V, Malvache A, Tressard T, Dupuy N, Cossart R (2015) Internally recurring hippocampal sequences as a population template of spatiotemporal information. Neuron. 88(2):357-66. doi: 10.1016/j.neuron.2015.09.052

Voloh B, Womelsdorf T (2016) A role of phase-resetting in coordinating large scale neural networks during attention and goal-directed behavior. Front Syst Neurosci 10:18. doi: 10.3389/fnsys.2016.00018

Wagatsuma A, Okuyama T, Sun C, Smith LM, Abe K, Tonegawa S. (2018) Locus coeruleus input to hippocampal CA3 drives single-trial learning of a novel context. Proc Natl Acad Sci (USA) 115(2):E310-E316. doi: 10.1073/pnas.1714082115.

Womelsdorf T, Schoffelen JM, Oostenveld R, Singe, W, Desimone R, Engel AK, Fries P. (2007) Modulation of neuronal interactions through neuronal synchronization. Science 316: 1609–1612. doi: 10.1126/science.1139597

Xiang L, Harel A, Gao H, Pickering AE, Sara SJ, Wiener SI. (2019) Behavioral correlates of activity of optogenetically identified locus cœruleus noradrenergic neurons in rats performing T-maze tasks. Sci Rep. 9(1):1361. doi: 10.1038/s41598-018-37227-w.

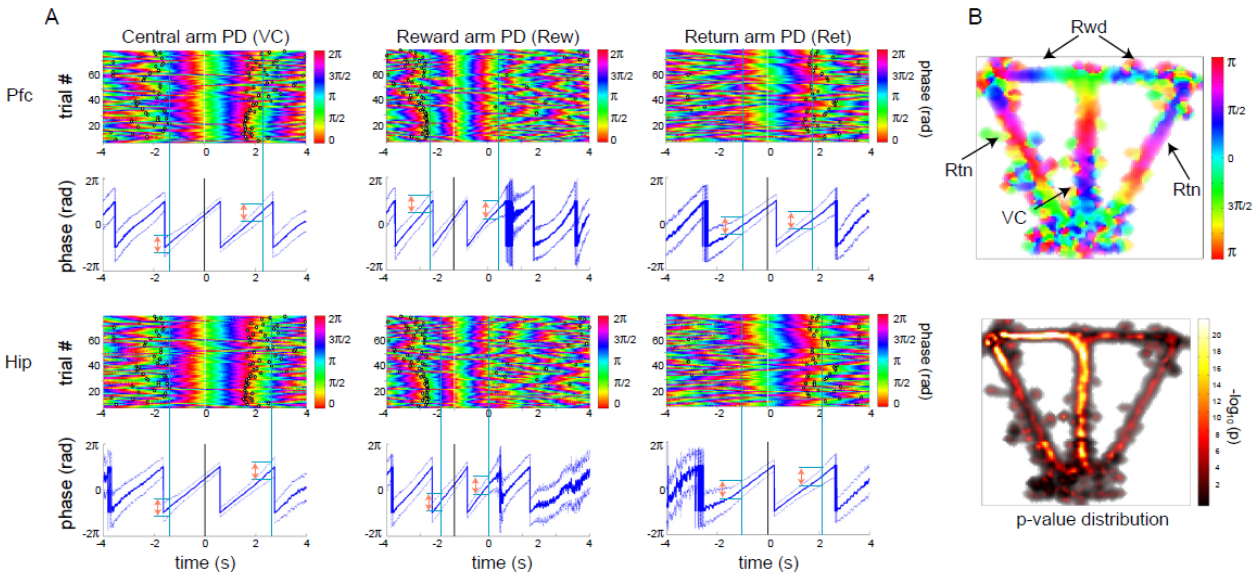

Supplementary Figure 1. The infra-slow cycles could continue through sequential phases from one task event to the following one. Plots are in same format as in Figure 4. A) Note that regular phase-locking in the left column (VC) starts prior to zero just after the Rtn PD (black dots prior to zero) and continues up to Rwd PD (black dots after zero). The other columns are comparable. B) Mean infra-slow phase distribution for this session (as in Fig. 2) also shows the continuity of the phase distribution on maze. Arrows show photodetector positions. (Note that colors indicating mean phase are different at the respective photodetector types). (Note that the color codes in the scales of A and B are not the same.)

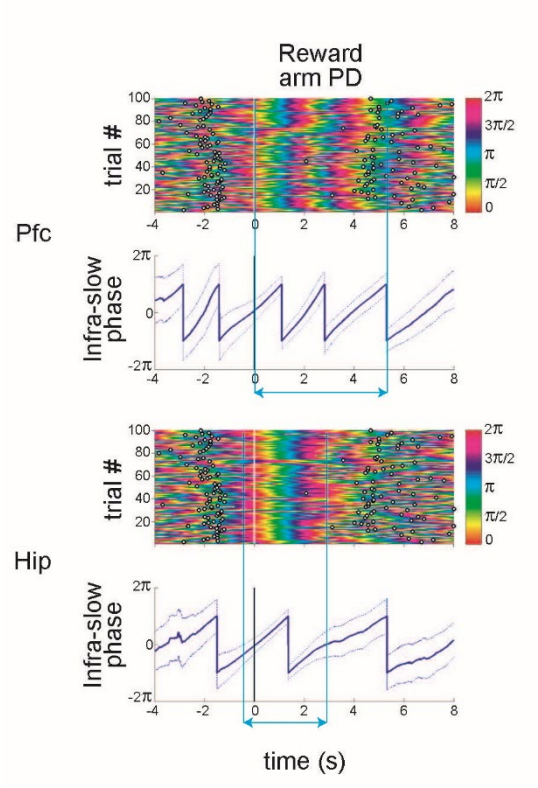

Supplementary Figure 2. Infra-slow rhythms recorded simultaneously in Hip and Pfc can have different cycle lengths. Note that regular phase-locking to Rwd extends for about 2.5 infra-slow cycles in Pfc, but only about 1 cycle for Hip. The durations of the cycles are about 2.1 s (corresponding to 0.48 Hz) for the first Pfc Rwd cycle, 1.9 s for the second (0.53 Hz), and 3.1 s for Hip Rwd (0.32 Hz). (Same format as Figure 4.)

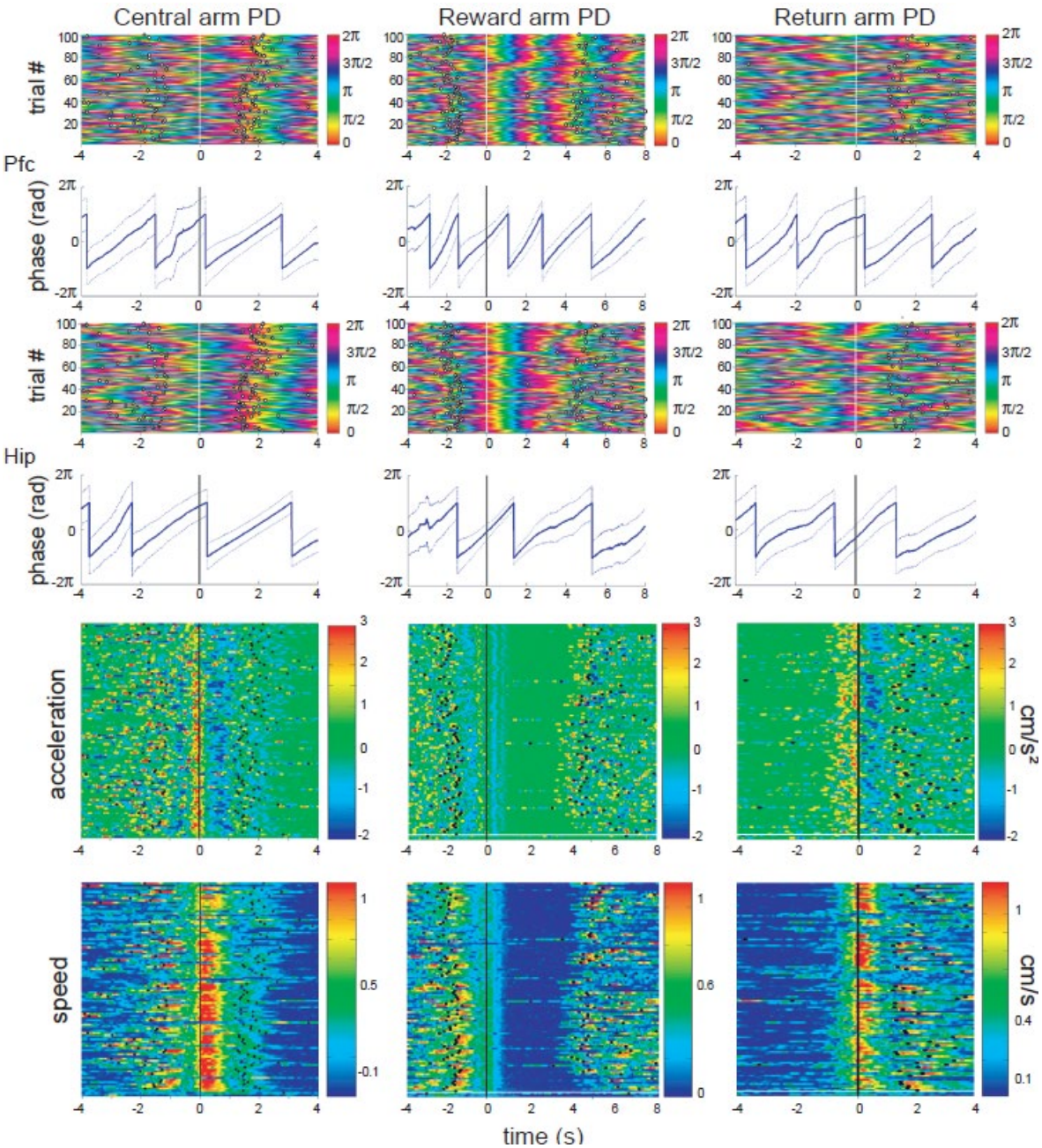

Supplementary Figure 3. Example of lack of a clear relation between speed, acceleration and infra-slow phase. Acceleration increases before central and return arm PD crossings,with speed increasing after. But, the phase is π radians for the former and -0.2*π radians for the latter.

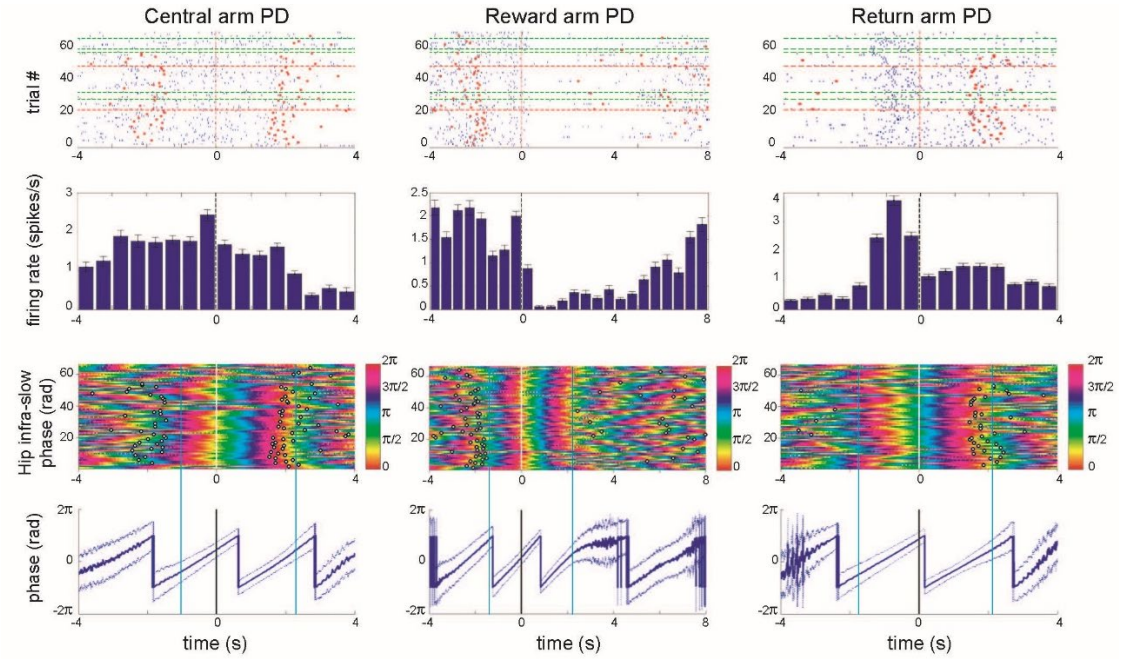

Supplementary Figure 4. Top) Example of LC neuron activity in relation to task events for the cell recorded in the session of Figure 4 (reproduced here). Red dots to the left of zero correspond to the previous task event, and those to the right indicate the timing of the subsequent event. Note that the regular phase-locking of infra-slow oscillations at the Reward arm PD continues in the interval (0 s, 2 s), while the LC neuron is inactive.

	# phase-locked neurons	resultant vector length (%)
Hip Slow	21	15.2±1.4
Pfc Slow	18	15.0±1.5
Hip Delta	11	8.2±0.8
Pfc Delta	15	9.7±0.7
Hip Theta	5	5.6±0.5
Pfc Theta	7	8.1±1.0
Hip Gamma	2	6.9±0.3
Pfc Gamma	2	7.5±1.0

Supplementary Table 1. Tallies of LC neurons phase-locked to LFP oscillations (Rayleigh test, $p<0.05$) in several frequency bands. The total population was 37 neurons. Resultant vector length were calculated only from neurons with significant phase-locking. From top to bottom, the bands correspond to 0.1-1 Hz, 1-4 Hz, 5-10 Hz, and 40-80 Hz.